Fuel 217 (2018) 306–319

Contents lists available at ScienceDirect

Fuel

journal homepage: www.elsevier.com/locate/fuel

Full Length Article

# Entrained flow gasification Part 1: Gasification of glycol in an atmospheric-pressure experimental rig

S. Fleck[a,*], U. Santo[a], C. Hotz[a], T. Jakobs[a], G. Eckel[c], M. Mancini[d], R. Weber[d], T. Kolb[a,b]

[a] Karlsruhe Institute of Technology (KIT), Institute for Technical Chemistry, Gasification Technology Department (ITC), Hermann-von-Helmholtz-Platz 1, 76344 Eggenstein-Leopoldshafen, Germany
[b] Karlsruhe Institute of Technology (KIT), Engler-Bunte-Institute, Division of Fuel Technology (EBI ceb), Engler-Bunte-Ring 3, 76131 Karlsruhe, Germany
[c] German Aerospace Center (DLR), Institute of Combustion Technology, Pfaffenwaldring 38-40, 70569 Stuttgart, Germany
[d] Clausthal University of Technology, Institute of Energy and Process Engineering and Fuel Technology (IEVB), Agricolastr. 4, 38678 Clausthal-Zellerfeld, Germany

ARTICLE INFO

*Keywords:*
Entrained flow gasification
Liquid fuel
Experimental data
Local profiles
Spray data
Data validation

ABSTRACT

Three coordinated papers are presented concerning entrained flow gasification of a liquid fuel under atmospheric conditions. The work is based on a detailed mapping of process parameters inside the entrained flow gasifier and at the gasifier outlet. In this paper the experimental setup and the experimental data are reported. Mono ethylene glycol (MEG) is used as a well-defined surrogate fuel for biogenic oils. The overall performance of the reactor is evaluated by measuring the gas-phase composition at the reactor outlet; radial profiles of gas-phase composition ($CO_2$, CO, $H_2$, $CH_4$, hydrocarbons) and temperature at 300 and 680 mm distances from the burner are measured to describe the mixing and reaction pattern in the gasifier. Global and local species balances are used to derive data that are not accessible by measurement. Characteristic parameters, i.e. stoichiometry, carbon conversion and water gas shift temperature, are derived to assess consistency of the measured data. Droplet size distribution and droplet velocity at the burner nozzle are reported based on atomization test rig experiments and direct measurements in the burner near field under gasification conditions. The experiments show a free jet with a strong outer recirculation zone as core gasification pattern. The measured species concentrations and temperatures provide an insight into both the mixing and the reactions in the burner near field. The water gas shift equilibrium is reached for a temperature of 1495 K upstream of the gasifier outlet. Hydrocarbons are not completely converted due to the low temperatures near the gasifier outlet.

The research work has been conducted within the research cooperation of the Helmholtz Virtual Institute HVIGasTech.

## 1. Introduction

Entrained flow gasifiers (EFG) dominate the gasification market worldwide [1,2]. The technology is suited for the production of a high quality syngas, with minimum amounts of hydrocarbons, tar and soot from solid and liquid fuels, as well as from suspension fuels (e.g. slurries consisting of a pyrolysis oil and a bio-char as applied in the bioliq® process [3]). The design and scale-up of EFG is mainly based on experience and to a lesser extent on a thorough understanding of the physical and thermo-chemical processes taking place in the gasifier. Especially for suspension fuels, the gasification process, as a three-phase high-temperature and high-pressure process, shows very complex interactions and overlapping of different physical and thermo-chemical process steps.

The researchers collaborating within the Helmholtz Virtual Institute for Gasification Technology, HVIGasTech [4], have focused on the development and validation of a numerical simulation tool for the mathematical description of the high-pressure entrained flow gasification process for suspension fuels. The tool is to be based on experimental data derived from both the atmospheric lab-scale gasifier (REGA) as well as the high pressure entrained flow pilot-scale gasifier of the bioliq® process [3]. The sub-models of the simulation tool describe the atomization of suspension fuels [5], the homogeneous and heterogeneous kinetics of the gasification of liquids and chars [6], the slag behavior [7] and the radiative heat transfer [8,9].

## 2. The physical and thermo-chemical sub-processes in entrained flow gasification of a suspension fuel

Entrained flow gasifiers processing liquid or suspension fuels

* Corresponding author.
*E-mail address:* sabine.fleck@kit.edu (S. Fleck).

https://doi.org/10.1016/j.fuel.2017.12.077
Received 14 May 2017; Received in revised form 15 December 2017; Accepted 18 December 2017
Available online 02 January 2018

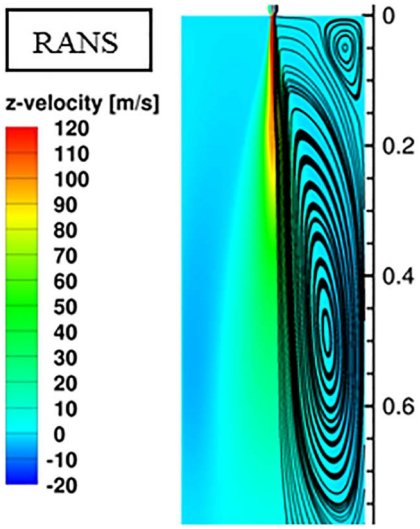


**Fig. 1.** Stream function from the RANS simulation for gasification of mono ethylene glycol in the atmospheric entrained flow gasifier [14].

(slurry) are typically equipped with twin-fluid atomizers. In the bioliq® process a suspension fuel which consists of pyrolysis oil and pyrolysis char from a fast pyrolysis process is converted to syngas in an entrained flow gasifier. The fuel is fed at a low velocity while the gasification medium is supplied at a significantly higher velocity to provide the required momentum for atomization. The burners may have different geometries especially with respect to the position of the fuel inlet; either central or annular nozzles are used and oxygen and steam are applied for atomization and gasification [10,11]. As the atomization process is driven by the momentum of the gasification medium, the overall stoichiometry in the gasifier, i.e. the oxygen/fuel ratio, is directly proportional to the gas-to-liquid ratio (GLR), which is a key parameter for the spray quality [12,13].

The flow pattern in an entrained flow gasifier is dominated by the high momentum of the gasification medium flow generating a highly turbulent enclosed jet. Within this jet the dominating physical and thermo-chemical sub-processes of entrained flow gasification take place. Fig. 1 shows both the streamlines and the axial velocities in an EFG from the RANS simulation [14], to underline the basic features of the flow. The high momentum gas jet drives an outer recirculation zone which carries hot syngas from the end of the gasification zone to the burner near field, where it reacts with the oxygen introduced as gasification and atomization medium, thus being responsible for the stabilization of the flame. The hot recirculated gases are entrained along the jet, affecting the temperature and species profiles in the jet zone.

In order to identify the physical and thermo-chemical process steps dominating entrained flow gasification Fig. 2 (left) depicts a typical droplet/particle trajectory pattern as derived from the numerical simulation of a slurry-fed EFG [12]. The colors of the trajectories represent different physical and thermo-chemical process steps which a fuel droplet experiences during the gasification process:

(a) **Atomization, heating-up, evaporation and decomposition** (light blue) of the liquid fuel releasing fuel vapors into the gas-phase.
(b) **Heating-up** and **pyrolysis** (orange) of the solid fuel particle (primary char) which is released from the slurry droplet. The volatiles are released into the gas-phase; the remaining solids are denoted as secondary char featuring different morphology and reactivity as compared to the original solid particle in the feed. The secondary char may also contain solids generated from the thermal degradation of the liquid-phase which may lead to the generation of cenospheres [6,15].
(c) **Gasification** (red) of the secondary-char, i.e. heterogeneous reactions of the secondary-char with steam and carbon dioxide [16].
(d) **Ash, slag-forming particles** (dark blue) impinging on the gasifier walls or leaving the gasifier with the syngas flow.

Fig. 2 (right) gives a detailed overview of the sequence of subprocesses and intermediate species relevant for EFG. The suspension fuel is atomized close to the burner nozzle within the highly turbulent gas jet which is enveloped by the gas flame burning recirculated syngas with oxygen at very high temperatures. The liquid fraction of the slurry evaporates; the vapors react with $O_2$, $CO_2$ and $H_2O$ while the solid fuel fraction (primary char) undergoes a secondary pyrolysis and penetrates as secondary char, or as cenospheres, through this highly reactive zone into the downstream gasification zone where the endothermal gasification of the solid fuel components takes place, determining the syngas quality and fuel conversion efficiency.

## 3. Literature review

Detailed data from entrained flow gasification experiments is rare in literature. This chapter gives an overview of experimental data found in literature. A detailed discussion is omitted here, as this is included in the second part of three coordinated papers [14]. In Japan, a 200 t/d pilot scale updraft gasifier was operated by Mitsubishi Heavy Industries (MHI) within an IGCC development project. The syngas composition at the reactor outlet and centerline temperatures were measured for operation at 27 bar with pulverized coal [17,18]. Guo et al. [19] studied the influence of O/C and steam/C ratio on the performance of an entrained flow gasifier operated at 10–30 bar, feeding pulverized coal by diametrically opposed burners in the upper part of the reactor. More detailed experimental investigations were carried out in lab-scale gasifiers. Harris et al. [20] used a 20 bar entrained flow reactor with electrically heated walls to study the influence of O/C ratio, residence time and coal type on fuel conversion and product gas composition. By inserting an oil-cooled probe from the bottom and adjusting the height of the probe, partially reacted char and gas were sampled at variable residence times and temperatures. At the lab scale atmospheric entrained flow gasifier operated at Brigham Young University (BYU) radial profiles of gas phase composition and temperature were measured. Applying a water quench probe for gas and particle sampling the influence of coal type, particle size and operating conditions on fuel conversion, local mixing and reaction processes were investigated [21–23].The experimental data derived from the MHI and BYU gasifiers was used for validation of several simulations [17,18,24–26]. Tremel et al. [27] studied the pyrolysis and gasification behavior of different coal types in the Pressurized High Temperature Entrained Flow Reactor PITER varying pressure, temperature and residence time. Volatile yield was determined applying nitrogen as carrier gas. Fuel conversion was determined under gasification conditions from the gas phase composition measured at the reactor outlet.

For biogenic fuels data exists for laboratory scale downdraft entrained flow gasifiers operated with oxygen, air or steam under atmospheric pressure. Qin et al. [28] and Hernandez et al. [29] both used atmospheric, externally heated entrained flow gasifiers to investigate the influence of operating conditions on fuel conversion of different pulverized biomasses by sampling gas and particles at the reactor outlet. The data from the gasifier operated at Technical University of Denmark (DTU) [28] was used for validation of different simulation models [30,31]. Several studies were concerned with gasification of black liquor. Sricharoenchaikul et al. [32] investigated the gasification characteristics of black liquor in a laboratory scale, laminar entrained flow reactor with heated wall. Syngas taken from the reactor outlet was analyzed by FTIR. Experimental investigation at larger scale was carried out by Carlsson et al. [33] and Weiland et al. [34] using a 3 MW pressurized entrained flow gasifier. Measuring the syngas composition at the reactor outlet, the effect of operating conditions was studied. The

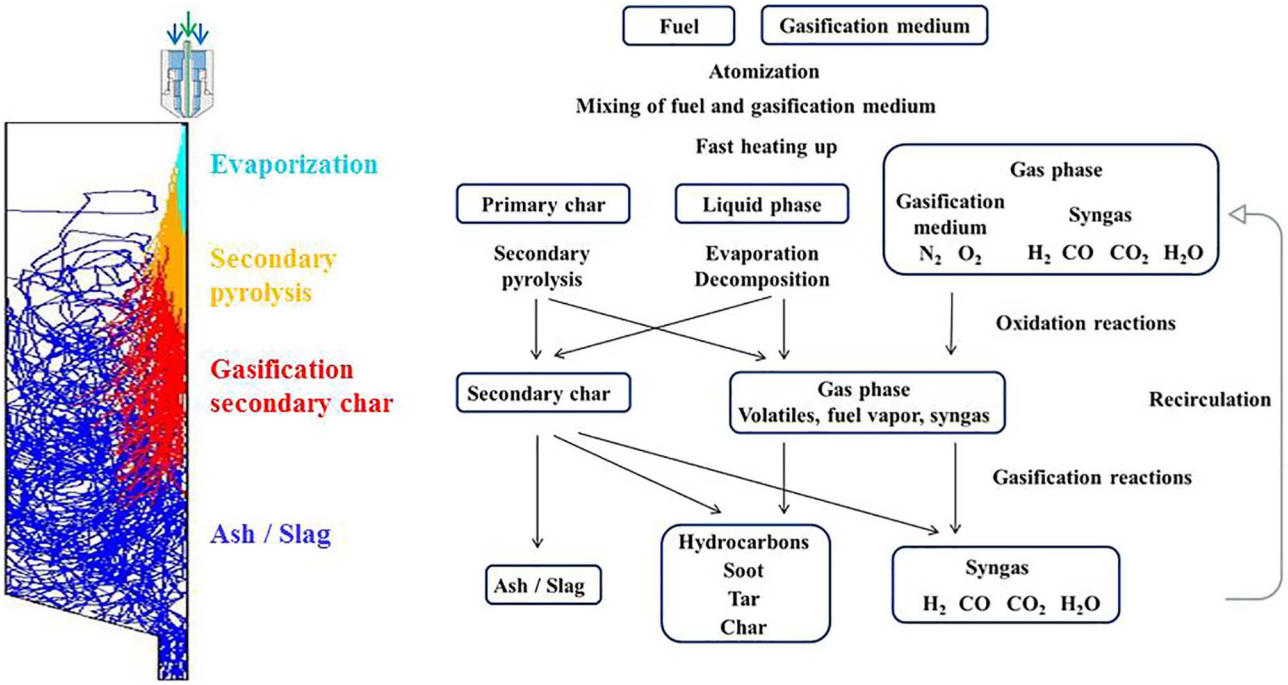


**Fig. 2.** Left: Trajectories and process steps of slurry droplets in an entrained flow gasifier [12]. Right: sub-processes and species relevant for entrained flow gasification of slurry.

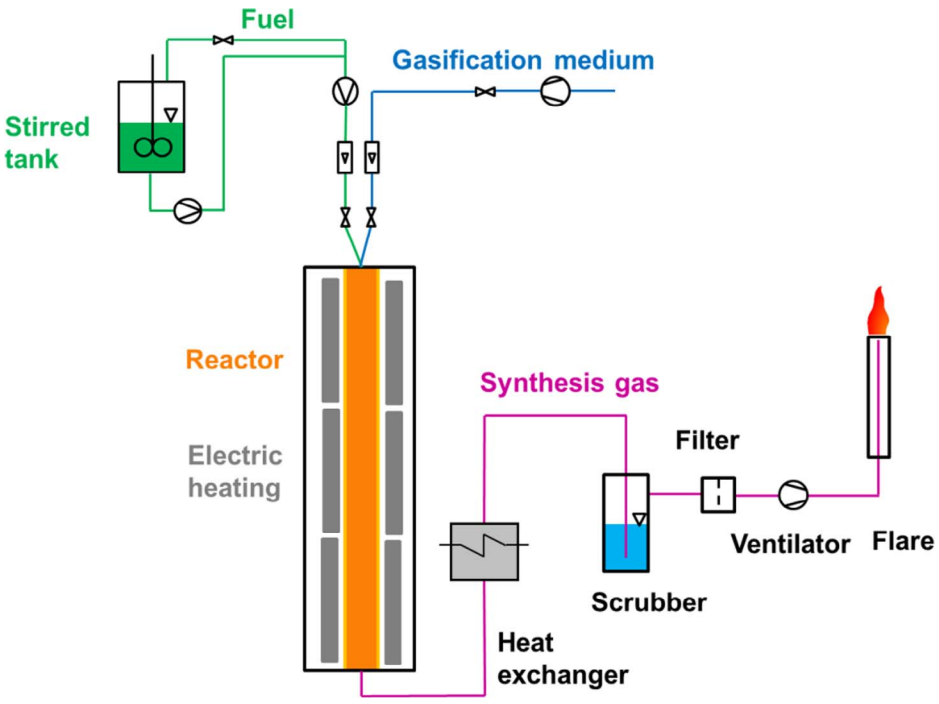


**Fig. 3.** Process flow scheme of the pilot scale entrained flow gasifier REGA.

data derived from the 3 MW black liquor gasifier also served for validation of simulation models [35,36].

## 4. Objectives

In order to put the simulation models on a sound basis, in the first step a sequence of gasification experiments are conducted starting off with atmospheric gasification of a liquid surrogate fuel (mono ethylene glycol – MEG), which facilitates set-up of the numerical models. MEG was chosen as its C/H/O ratio and heating value are comparable to that of biomass based pyrolysis oils. A set of three coordinated papers is presented with a detailed report on the gasification experiments provided in this paper. The other two papers are on numerical simulations of the gasification experiments; the first presenting RANS simulations [14],while the second one reporting on LES [37]. In this way the input data for the numerical simulations are provided by the experimental team, and the results of the numerical simulation are validated against in-gasifier data. The experimental run described in this paper, and considered in the associated papers, is named as REGA-glycol-T1 data set.

In the second step atmospheric gasification of a suspension fuel (bio-slurry) will be treated in the same way, with special focus on the heterogeneous gasification of biogenic chars. In the third step the RANS and LES models will then be applied to describe the gasification

experiments conducted in the high-pressure entrained flow gasifier of the bioliq® pilot plant. In this semi-technical (5 MW/40 bar) entrained flow gasifier the experimental data are not as detailed as in the atmospheric experiments, but the overall gasifier performance, based on detailed mass/species and energy balances can be compared with the simulation results. With this approach a thoroughly validated numerical simulation tool for the design and scale-up of high-pressure entrained flow gasifiers will be developed.

## 5. Facilities and measuring techniques

### 5.1. Research entrained flow gasifier (REGA)

Gasification experiments were carried out in the atmospheric Research Entrained flow GAsifier (REGA). The REGA process flow sheet is shown in Fig. 3. The main parts of the test rig are: the fuel and gasification medium supply, the reactor with analytical equipment, the syngas cooler, the scrubber and the flare for combustion of the off-gas. Liquid and suspension fuels are stored in a stirred tank with outer circulation to avoid sedimentation of particles. The storage tank and the circuit can be heated up to a maximum temperature of 80 °C to adjust the viscosity of the fuels. The fuel, together with the gasification medium, is fed to the burner which is equipped with a twin fluid external mixing atomizer [12]. Oxygen-enriched dry pressurized-air is used as gasification/atomization medium. The amount of oxygen in the gasification medium can be varied in the range of 21 to 70 vol%. The limitation to 70 vol% is due to safety reasons. The heat loss of the system is minimized by electric heating of the reactor walls.

REGA is operated at 60 kW fuel input which, for the mono ethylene glycol, corresponds to a feed rate of 13 kg/h and around two seconds of average residence time (for a syngas flow rate of 60 $m^3$/h (STP), average gas temperature of 1473 K and a reactor volume of 0.9 $m^3$). Fig. 4 depicts an axial cut through the gasification reactor with detailed reactor inlet and outlet as well as the twin fluid external mixing atomizer. The reactor consists of a ceramic tube with an inner diameter of 0.28 m and a length of 3 m. Ceramic shielded type S thermocouples ($T_1$ to $T_7$) are installed at fixed positions along the reactor axis to monitor the axial gas temperature profile during operation. The reactor is equipped with flanges along the reactor axis for sampling probes and thermocouples access. For laser-based measurements the flanges can be equipped with sight glasses which are purged with nitrogen. The burner is mounted at the top of the reactor. By means of a vertically movable burner construction the burner position can be shifted in axial direction. Thus, measurements can be taken at any distance from the atomizer, enabling complete data mapping of the reactor.

**Table 1**
Accuracy of input streams (fuel, gasification medium, purge flow) according to manufacturer information.

| Species | Measurement range | Accuracy of set point values |
|---|---|---|
| Fuel (MEG) | 0–20 kg/h | 12.56 ± 0.04 kg/h |
| Air | 0–20 $m^3$/h (STP) | 7.03 ± 0.04 $m^3$/h (STP) |
| Oxygen | 0–20 $m^3$/h (STP) | 4.97 ± 0.04 $m^3$/h (STP) |
| Nitrogen | 0–4.2 $m^3$/h (STP) | 0.51 ± 0.004 $m^3$/h (STP) |

STP = standard temperature and pressure (273 K, 1 bar).

The fuel mass flow rate is measured by a Coriolis mass flow meter, while the volume flow rates of the gasification medium, air and oxygen, as well as the purge nitrogen are determined by thermal flow controllers based on hot wire anemometry. The accuracy of the measurements is given in Table 1.

Gas samples are extracted from the reactor using cooled steel probes with a ceramic tip. The samples are quenched by thermal oil at 80 °C to prevent further reactions in the sampling line. The gas samples are filtered; a part is cooled to 3 °C and then analyzed for the dry concentrations of CO, $CO_2$, $H_2$, $O_2$ and $CH_4$ in standard gas analyzers. The $N_2$ content is determined by difference. Organic carbon ($C_{org}$) is measured in the wet gas using a Flame Ionization Detector (FID) operated at 160 °C.

Table 2 lists the measurement principles [38] used for gas analysis as well as the accuracies of the measured values. All the measurement results are influenced by the uncertainty of the analyzer signal, which is

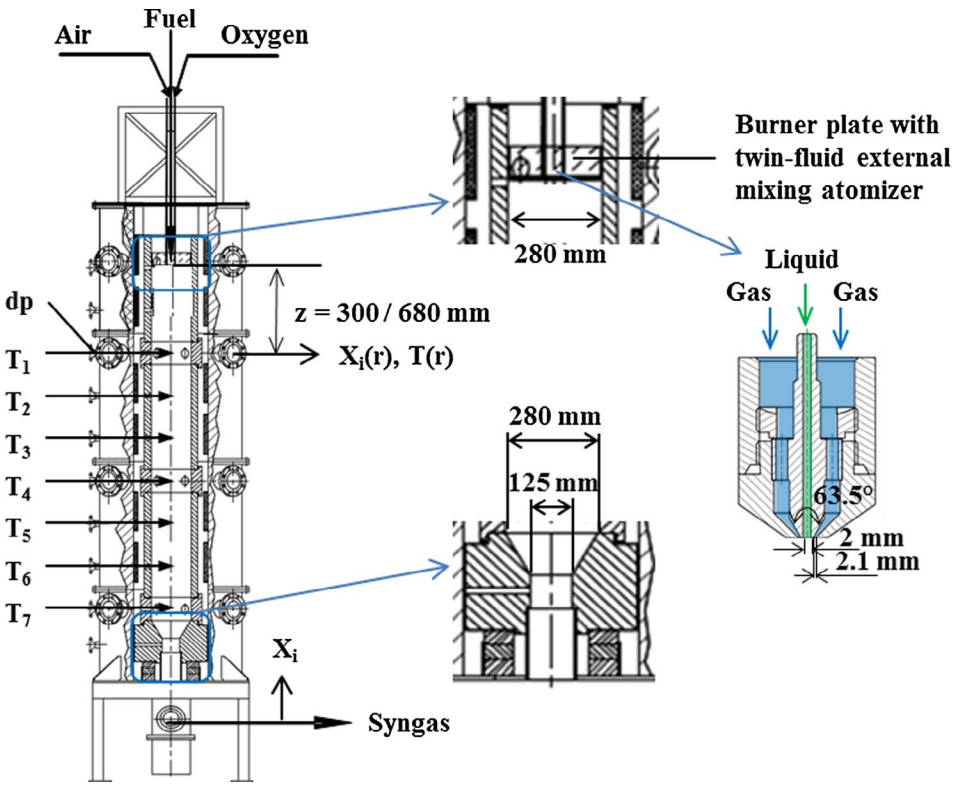


**Fig. 4.** Axial cut through the gasification reactor with detailed reactor inlet, outlet and twin-fluid external mixing atomizer.

**Table 2**
Principle and accuracies of gas-phase measurements.

| Species | Principle | Measurement range/vol% | Accuracy of reference gas/vol% | Accuracy of analyzer signal/ vol% |
|---|---|---|---|---|
| $H_2$ | Thermal conductivity | 0–50 | ± 0.39 | ± 0.25 |
| CO | NDIR | 0–50 | ± 0.46 | ± 0.10 |
| $CO_2$ | NDIR | 0–30 | ± 0.44 | ± 0.06 |
| $CH_4$ | NDIR | 0–10 | ± 0.002 | ± 0.02 |
| $O_2$ | Paramagnetism | 0–15 | | ± 0.08 |
| $C_{org}$ | FID | 0–10 g/m$^3$ | | ± 50 mg/m$^3$ |

(according to manufacturer) 0.2 % of the measurement range for CO, $CO_2$ and $CH_4$ and 0.5 % of the measurement range for $H_2$, $O_2$ and $C_{org}$. Especially the measurements of CO and $CO_2$ by NDIR sensors are influenced by cross sensitivities. In order to eliminate this effect the analyzers were calibrated using reference gases with a composition comparable to the syngas. Thus, the inaccuracy of the measurements is reduced to the uncertainty of the concentrations of dry gas species in the reference gas of ± 2 vol% (relative).

Radial temperature profiles are measured using type B double bead thermocouples. In order to minimize the radiation effects double bead thermocouples with bead diameters of 300 and 1500 µm are used. The measured values are corrected for radiation assuming a wall temperature of 1473 K [39].

Both the droplet velocities and diameter are measured using the standard PDA system. Optical accessibility of the gasifier allowed only a backward scattering arrangement applying a lens with 1000 mm focal length.

### 5.2. Atmospheric spray test rig (ATMO)

The twin fluid atomizer applied in the REGA experiments (see Fig. 4) was characterized using the atmospheric spray test rig ATMO. The process flow scheme of the spray test rig is shown in Fig. 5. The atomizer is mounted on the twin fluid lance which is equipped with a liquid and a gas supply. Pulsation-free liquid supply is guaranteed by using a pressurized vessel. Liquid mass flow is measured by a Coriolis

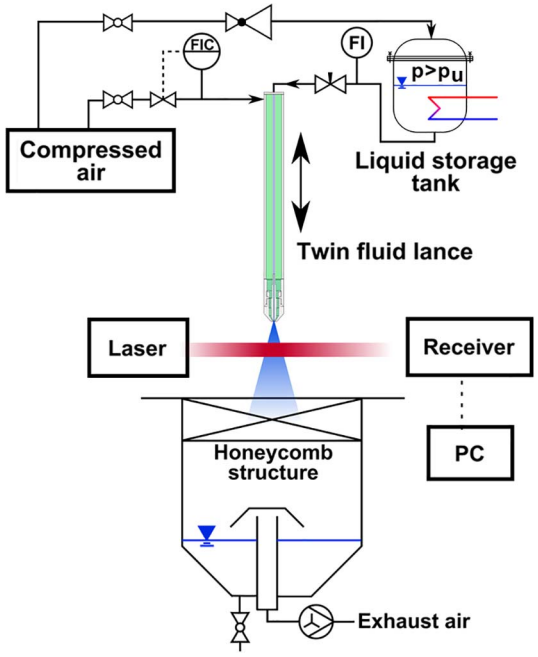


**Fig. 5.** Process flow scheme of the spray test rig ATMO.

mass flow meter and can be adjusted in the range of 5–50 kg/h. Pressurized air is used as atomization medium. The gas-to-liquid ratio (GLR) can be varied in the range of 0.5–2.

Atomization experiments were performed using the fuel applied at REGA (mono ethylene glycol, see Section 7.1) as liquid and compressed air as atomization medium. A high speed camera was employed for investigation of spray angle and jet breakup in the near atomizer region. The camera featured a maximum resolution of 1024 × 1024 pixel at a frame rate of 3.6 kHz, for detailed description of the camera setup see [40]. A 2-D-Fiber PDA System was operated in forward scattering arrangement in the 1st order refraction mode for detection of drop size and velocity [41]. The receiver was set to an off-axis angle of 30°. In order to ensure a high data rate and quality, a 200 µm slit was used to reduce the length of the measurement volume. Both, transmitter and receiver were equipped with a lens of 500 mm focal length. In order to optimize the PDA instrument settings towards small droplets, e.g. data rate and data validation rate, the PDA user settings were adjusted based on a sensitivity study [42]. Sending and receiving optics were mounted on a traverse system to guarantee reproducible and accurate positioning. Data were obtained by moving the PDA-detection relatively to the atomizer position at an axial distance of 50 mm to the atomizer orifice varying the radial position in the range of $-15\,\text{mm} < r < 15\,\text{mm}$ with a step of 5 mm. The raw data from the manufacturer software were used to compute arithmetic means by using an in-house spray characterization toolbox SprayCat.

## 6. Reactor balancing and consistency of experimental data

Experimental research is prone to data uncertainty. Experimental data are often not completely available for process balancing and data plausibility check. We have put a great emphasis on both REGA balancing and checking the consistency of the measured data. We clearly differentiate between directly measured data and data derived from the measured values.

Under ideal process conditions the products of gasification are the syngas components CO, $CO_2$, $H_2$ and $H_2O$. The composition of the syngas can be calculated from the molecular composition of the feed (fuel plus gasification media) and the gas temperature if water gas shift (WGS) equilibrium [43] (Eq. (1)) is assumed and all side products can be neglected.

$$CO + H_2O \leftrightarrows CO_2 + H_2 \quad \Delta_R H = -41\ \text{kJ/mol} \tag{1}$$

In technical systems, complete fuel conversion may not be achievable due to non-ideal process conditions like incomplete mixing of fuel and gasification medium and insufficient residence time and/or temperature for the fuel conversion process. Intermediates from decomposition and conversion of liquid and solid fuel components will be found at the reactor outlet, influencing the syngas quality and the energy efficiency of the process. However, for the main syngas components (CO, $CO_2$, $H_2$, $H_2O$) water gas shift reaction equilibrium (Eq. (1)) may be assumed as partial equilibrium, especially for entrained flow gasification with typically high reactor temperatures [33].

The main intermediates at high gasification temperatures are hydrocarbons (primarily methane), soot and char [44,45]. In the experimental work presented, $CH_4$ and the sum of volatile hydrocarbons with a condensation point above 160 °C (temperature of FID analyzer) are measured and both are taken into consideration for the interpretation of the results. For the process conditions chosen (see Section 7.1) it is reported in literature, that no hydrocarbons besides $CH_4$ are to be expected at the reactor outlet [46,47].

### 6.1. Balancing of the REGA gasifier

Fig. 6 shows the REGA reactor with the boundary for global balancing. The measured data are marked in green, the derived data in pink.

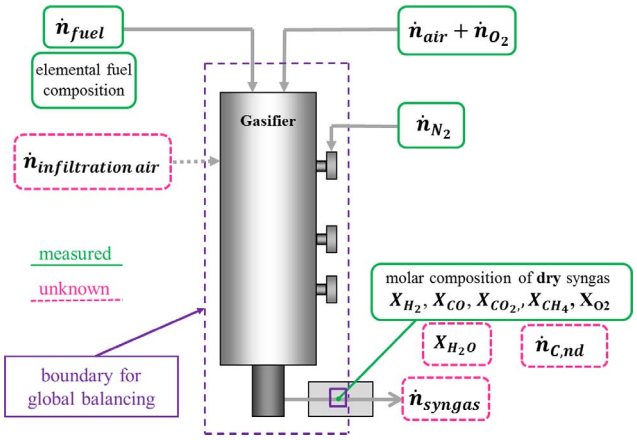


**Fig. 6.** REGA reactor with input and output variables (green/continuous line = measured, pink/dotted line = unknown values) and boundary for global balancing. (For interpretation of the references to colour in this figure legend, the reader is referred to the web version of this article.)

Molar flow rates of species C, H, O and N (see Eqs. (2) to (5)) are balanced using the fuel analysis, the measured flow rates of the feed streams and the measured dry syngas composition ($H_2$, CO, $CO_2$, $CH_4$). $\dot{n}_i$ is the malar flowrate of species i in mol/unit time. The following assumptions are made:

- in the gas phase only CO, $CO_2$ and $CH_4$ are considered as carbon containing species
- carbon balance is closed using a molar H/C ratio of 0.8 for not detected carbon containing molecules
- $N_2$ is the only N-species in the syngas

Carbon balance:

$$\dot{n}_{C,fuel} = \dot{n}_{C,syngas} + \dot{n}_{C,nd} = \dot{n}_{syngas}\cdot(X_{CH4,dry} + X_{CO,dry} + X_{CO2,dry})\cdot(1-X_{H_2O}) + \dot{n}_{C,nd} \quad (2)$$

Hydrogen balance:

$$\dot{n}_{H,fuel} = \dot{n}_{syngas}\cdot((4X_{CH4,dry} + 2\cdot X_{H2,dry})\cdot(1-X_{H_2O}) + 2\cdot X_{H_2O}) + 0.8\cdot\dot{n}_{C,nd} \quad (3)$$

Oxygen balance:

$$\dot{n}_{O,fuel} + 2\cdot\dot{n}_{O_2} + 2\cdot 0.21\cdot(\dot{n}_{air} + \dot{n}_{infiltration\ air}) = \dot{n}_{syngas}\cdot((X_{CO,dry} + 2\cdot X_{CO_2,dry} + 2\cdot X_{O_2,dry})\cdot(1-X_{H_2O}) + X_{H_2O}) \quad (4)$$

Nitrogen balance:

$$\dot{n}_{N,fuel} + 2\cdot\dot{n}_{N2,purge} + 2\cdot 0.79\cdot(\dot{n}_{air} + \dot{n}_{infiltration\ air}) = \dot{n}_{syngas}\cdot 2\cdot X_{N_2,dry}\cdot(1-X_{H_2O}) \quad (5)$$

$$X_{N_2,dry} = 1-(X_{H_2,dry} + X_{CO,dry} + X_{CO_2,dry} + X_{CH_4,dry}) \quad (6)$$

Aspen equilibrium calculations based on the measured input data and the above listed assumptions showed a good agreement with the measured gas-phase composition (see Section 7.3).

Four unknown parameters are derived from the balances:

- flow rate of infiltration air $\dot{n}_{infiltration\ air}$ (resulting from operation at a pressure 1 to 2 mbar below ambient)
- concentration of $H_2O$ in syngas at reactor outlet ($X_{H_2O}$)
- flow rate of syngas $\dot{n}_{syngas}$
- flow rate of not detected carbon ($\dot{n}_{C,nd}$)

The same procedure can be applied for a local volume element in the reactor at a certain radial and axial position using local measurements of the gas-phase composition. Assuming

- complete evaporation and decomposition of the fuel,
- complete mixing of the fuel and the gasification media,

the missing local values for $X_{H_2O}$, $\frac{\dot{n}_{syngas}}{\dot{n}_{fuel}}$, $\frac{\dot{n}_{infiltration\ air}}{\dot{n}_{fuel}}$ and $\dot{n}_{C,nd}$ can be calculated using the local concentration data.

### 6.2. Parameters for characterization of processes in the gasifier

Using both the reactor input data and the above formulated balances of C, O, H, N a number of characteristic parameters can be derived to describe mixing and reaction conditions in the gasifier. In this work the absolute stoichiometric ratio ($\lambda_{abs}$), the carbon conversion (CC) and the corresponding temperature of partial WGS equilibrium ($T_{WGS}$) are derived as global values at the reactor outlet, and as local values at a defined position in the reactor, to describe the gasification process quantitatively.

#### 6.2.1. Absolute stoichiometric ratio ($\lambda_{abs}$)

In general, the stoichiometric ratio λ is defined as the oxygen supply divided by the oxygen demand required for complete oxidation of the fuel.

$$\lambda = \frac{\dot{n}_{Oxygen\ supply}}{\dot{n}_{Oxygen\ stoich}} \quad (7)$$

The stoichiometric ratio $\lambda_{tech}$ is calculated using the composition ($C_xH_yO_z$) and the flow rates of fuel ($\dot{n}_{fuel}$) and oxidation medium ($\dot{n}_{O_2,supply}$). The reaction equation for stoichiometric combustion (Eq. (8)) of a fuel with a molar composition expressed as $C_xH_yO_z$ leads to the definition of $\lambda_{tech}$ shown in Eq. (9):

$$C_xH_yO_z + \left[x + \frac{y}{4} - \frac{z}{2}\right]\cdot O_2 \rightarrow x\cdot CO_2 + \frac{y}{2}\cdot H_2O \quad (8)$$

$$\lambda_{tech} = \frac{\dot{n}_{O_2,supply}}{\dot{n}_{fuel}\cdot(x + \frac{y}{4} - \frac{z}{2})} \quad (9)$$

The stoichiometric oxygen demand of the fuel is calculated from the elemental fuel composition, thus the oxygen contained in the fuel reduces the oxygen demand for stoichiometric conversion.

In general $\lambda_{tech}$ gives qualitative information only about fuel rich or oxygen rich conditions for the fuel conversion process. For fuels containing no oxygen (z = 0), which is a good approximation for fossil fuels, $\lambda_{tech}$ also describes correctly the oxidation state of the product gas mixture. In this context, oxidation state defines the part from complete oxidation, i.e. CO2 is oxidized completely (oxidation state 1), whereas CO is oxidized half (oxidation state 0.5). For biogenic fuels with a high oxygen content $\lambda_{tech}$ cannot be applied to calculate the oxidation state of the products. A simple example may illustrate the point: with CO as fuel and a partial oxidation reaction according to Eq. (10) the value for $\lambda_{tech}$ is 0.5; the oxidation state of the product gas mixture however is 0.75, as $CO_2$ is oxidized completely (oxidation state 1) whereas CO is in the oxidization state 0.5 with an overall oxidation state of 0.75 for the product gas mixture.

$$2CO + \frac{1}{2}O_2 \rightarrow CO + CO_2 \quad (10)$$

From these considerations we define an absolute $\lambda_{abs}$ according to Eq. (11):

$$\lambda_{abs} = \frac{n_O}{2\cdot n_C + 0.5\cdot n_H} \quad (11)$$

(with $n_i$ as number of moles of component i in the considered volume; this can be the burner inlet, a volume in the reactor and also at the reactor outlet, always describing the absolute stoichiometry at this position)

For our example, according to Eq. (10), $\lambda_{abs}$ equals 0.75 and thus describes both the stoichiometry and the oxidation state of the process

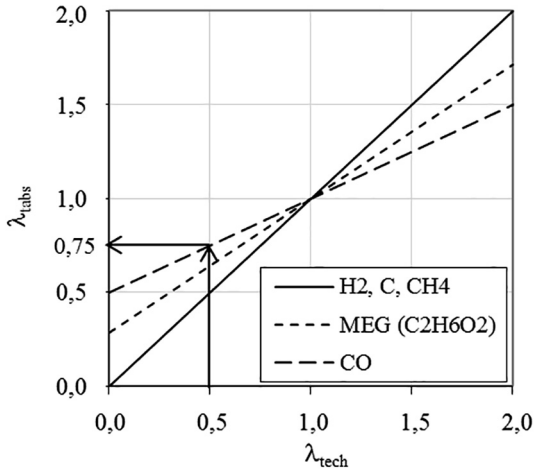


**Fig. 7.** Correlation of $\lambda_{tech}$ and $\lambda_{abs}$ for different fuels (the arrows mark the values for the example of sub-stoichiometric oxidation of CO).

correctly for any fuel. Fig. 7 shows the relationship between $\lambda_{tech}$ and $\lambda_{abs}$ for fuels with different oxygen content. It is obvious that both definitions for λ match at the stoichiometric point λ = 1. They match for fuels with z = 0 (no oxygen in fuel) at any stoichiometry but only $\lambda_{abs}$ describes the stoichiometry correctly for any fuel specification at any stoichiometry. Comparing the curves for CO and $C_2H_6O_2$ shows that with increasing oxygen content of the fuel, the deviation between $\lambda_{tech}$ and $\lambda_{abs}$ increases as well.

As for $\lambda_{tech}$, the global $\lambda_{abs}$ can be derived from fuel composition and feed flow rate of fuel and oxidation medium (see Eq. (12)), however carbon and hydrogen introduced with the fuel and the oxidation medium, have an oxygen demand in the denominator whereas oxygen in fuel and oxidation medium are assumed as oxygen supply in the numerator.

$$\lambda_{abs} = \frac{\dot{n}_{O_2,supply} + \dot{n}_{fuel}\cdot\frac{z}{2}}{\dot{n}_{fuel}\cdot(x + \frac{y}{4})} \tag{12}$$

$\lambda_{tech}$ is only defined at the reactor inlet and cannot describe the stoichiometric distribution in the reactor due to mixing. $\lambda_{abs}$, however, may also be calculated using local species concentrations at any position in the reactor, producing a local stoichiometry of the gas-phase as $\lambda_{abs,\ local}$. The difference between the global and the local $\lambda_{abs}$ is then used to describe the local reaction conditions in the gasifier, that is the state of mixing of fuel and oxidizer, the state of fuel conversion and local infiltration air ratio.

In our work $\lambda_{abs,local}$ is calculated using Eqs. (11) and (13) to (15) as the gas concentrations are available from measurement (CO, $CO_2$, $H_2$, $CH_4$) and balancing ($H_2O$).

$$\dot{n}_O = \dot{n}_{syngas}\cdot(2\cdot X_{O_2} + X_{CO} + 2\cdot X_{CO_2} + X_{H_2O}) \tag{13}$$

$$\dot{n}_C = \dot{n}_{syngas}\cdot(X_{CO} + X_{CO_2} + X_{CH_4}) \tag{14}$$

$$\dot{n}_H = \dot{n}_{syngas}\cdot(2\cdot X_{H_2O} + 2\cdot X_{H_2} + 4\cdot X_{CH_4}) \tag{15}$$

Only if all fuel components are converted into the gas species and the mixing between the gasification medium and the fuel is complete $\lambda_{abs,local}$ is equal to $\lambda_{abs,global}$. Either fuel missing in the gas phase (due to incomplete vaporization or mixing), existence of undetected intermediates (tar, char, hydrocarbons besides $CH_4$) or local infiltration air lead to the case $\lambda_{abs,\ local} > \lambda_{abs,\ global}$. If local fuel rich zones (due to incomplete mixing) are present we find $\lambda_{abs,local} < \lambda_{abs,global}$. Under sub-stoichiometric conditions an increase in $\lambda_{abs}$ results in a temperature increase. We therefore use the qualitative interdependence of local profiles of $\lambda_{abs,local}$ and temperature to check consistency of our experimental data.

#### 6.2.2. Carbon conversion (CC)

Carbon conversion is defined as the ratio of carbon detected in the gas-phase (as CO, $CO_2$ and $CH_4$) to the carbon fed into the reactor.

$$CC = \frac{Carbon\ detected\ in\ gas\ phase}{Carbon\ in\ feed} \tag{16}$$

For the REGA experiments and a fuel with the composition $C_xH_yO_z$ CC is calculated using Eq. (17), a similar definition is used by Vejahati [48] and Cousins [49].

$$CC = \frac{\dot{n}_{syngas}\cdot(X_{CO} + X_{CO_2} + X_{CH_4})}{\dot{n}_{fuel}\cdot x} \tag{17}$$

The carbon conversion can be calculated as a local value, as well as a global value at the reactor outlet using the concentration measurements and the C, H, O, N balances. For CC calculation the C/H/O/N composition is assumed to be equal to the reactor inlet conditions, this means that complete mixing of fuel and gasification medium is assumed at any position in the gasifier. This is correct at the reactor outlet; therefore $CC_{global}$ gives a reliable information on total carbon conversion in the gasifier. For the local CC values, the above assumption may not be correct for all positions in the gasifier. It is invalid for example in the spray zone, where local fuel rich or fuel lean zones exist due to evaporation and degradation of liquid fuel droplets. In this case, $CC_{local}$ is not a measure of carbon conversion but gives, together with the local stoichiometry, information about mixing and distribution of fuel, oxidizer and syngas components.

#### 6.2.3. Water gas shift temperature ($T_{WGS}$)

Under the assumption of water gas equilibrium, both the equilibrium constant $K_{P,WGS}$ and the equilibrium temperature [43] can be calculated from local species concentrations (see Eq. (18)). In this work, the relationship (see Eq. (19)) between $T_{WGS}$ and $K_{p,WGS}$ was derived using GRI3.0 mechanism [50] to ensure consistency with the modelling papers [14,37].

$$K_{P,WGS}(T) = \frac{X_{CO_2}\cdot X_{H_2}}{X_{CO}\cdot X_{H_2O}} \tag{18}$$

$$T_{WGS}(GRI3.0) = 8.142\cdot e^{-5.603\cdot log10(K_{p,WGS})} + 1084\cdot e^{-0.6516 log10(K_{p,WGS})} \tag{19}$$

Using the above procedure radial profiles of the water gas shift equilibrium temperature $T_{WGS}$ are derived and compared with measured temperature profiles (see Section 7). If WGS equilibrium is reached, the measured temperature is equal to the calculated $T_{WGS}$. In zones where substantial heat losses occur, i.e. near the reactor outlet and in the recirculation zone near the REGA walls, the measured temperature is expected to be lower than the calculated since $T_{WGS}$ corresponds to the temperature at which the WGS-equilibrium is 'frozen'. The influence of local dilution through $N_2$ purge streams imposing a cooling effect can also be identified upon comparing the measured temperature with the calculated $T_{WGS}$.

In zones with steep local concentration gradients (e.g., due to fuel evaporation or pyrolysis) a difference between the measured temperature and the calculated $T_{WGS}$ is to be expected. In all other regions of the gasifier, especially if temperatures above 1570 K are measured, $T_{WGS}$ can be used to examine consistency of the local temperature measurement.

### 6.3. Influence of measurement accuracy on characteristic parameters

The influence of inaccuracies in the measured data on the previously defined parameters ($\lambda_{abs}$, CC, $T_{WGS}$) is quantified by a sensitivity analysis. The considered data includes the fuel feed stream, the oxygen volume flow rate and the concentration of the main species in the syngas. In Fig. 8 the deviation of the characteristic parameters ($\lambda_{abs,local}$, CC and $T_{WGS}$) resulting from inaccuracy of the data is depicted. CO represents the gaseous species. $\lambda_{abs,local}$ is not very sensitive

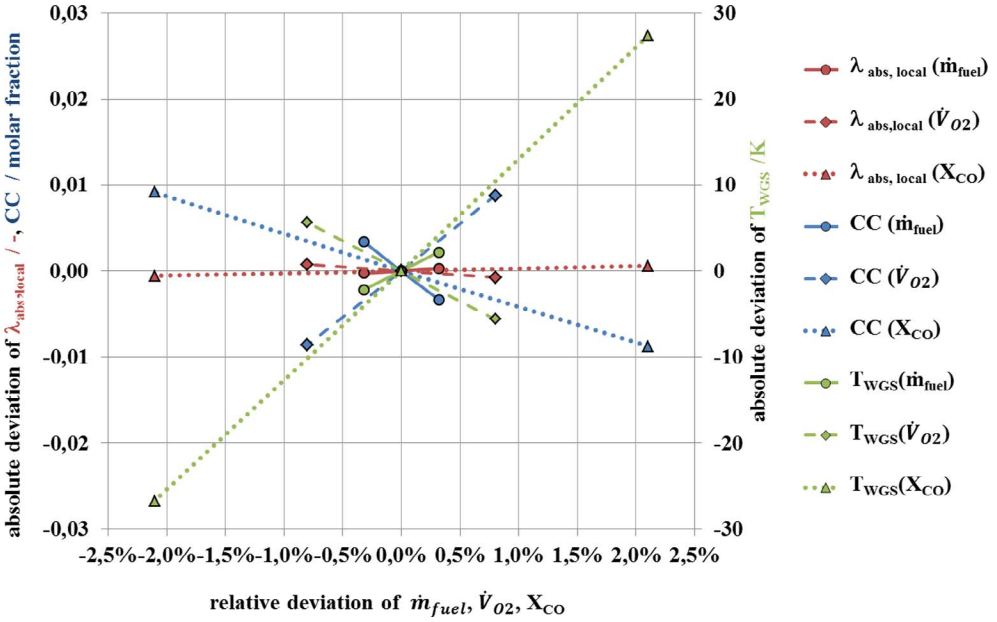


**Fig. 8.** Absolute deviation of characteristic parameters $\lambda_{abs,local}$, CC, $T_{WGS}$ due to measuring inaccuracies of $\dot{m}_{fuel}$, $\dot{V}_{O_2}$ and $X_{CO}$.

to the measured data, whereas $T_{WGS}$ and especially CC are significantly influenced by variations of the input streams. Thus, $\lambda_{abs,local}$ is particularly suitable to describe the processes in the reactor, for example to identify zones of incomplete mixing or oxidation zones. The CC parameter gives at least a qualitative information about the local fuel conversion situation.

## 7. Experimental and validation results

In this section the experimental run called REGA-glycol-T1 is described. The description includes (a) set point data for gasification experiments, (b) data from spray characterization under ambient and gasification conditions, (c) global characterization of the gasifier, (d) in-gasifier data describing the processes in the main reaction zone.

### 7.1. Operating conditions (set point)

As shown in Section 2 slurry gasification is a complex system with complex interactions of different physical and thermo-chemical processes. In order to improve the understanding of the single processes and facilitate a set-up of the numerical models, the complexity was reduced by using a liquid surrogate fuel with accurately defined composition. For the experiments reported here a high temperature level was chosen to suppress extensive formation of methane. Mono ethylene glycol was applied as surrogate fuel as its C/H/O ratio and heating value are comparable to that of biomass based pyrolysis oils [51,52]. The elementary composition of both fuels is compared in Table 3.

The set point values for the experiments (REGA-glycol-T1) were calculated applying the Aspen equilibrium model of the gasifier in combination with design specifications. The desired values of the adiabatic temperature (reaction kinetics), the exit velocity of the gasification medium (atomization) and the volume flow rate of syngas (residence time) were reached by adjusting the operational parameters (mass flow rate of fuel, stoichiometry and oxygen content of the gasification medium). The set point values for the gasification and atomization tests are listed in Table 4, for the atomization tests the mass flow rates of fuel, oxygen and air are relevant only.

### 7.2. Spray characterization

The performance of the burner nozzle was quantified in the ATMO spray test rig with atomizer inputs (pressures, flow rates and velocities) identical to the REGA gasification experiments, see Table 4. Fig. 9 shows the primary jet breakup and droplet formation within 50 mm distance downstream the nozzle orifice. The liquid jet is disintegrated directly at the nozzle orifice, the breakup mode can be described as fiber type, according to [53]. Spray angle was determined to be approximately 21°.

Realizing that the jet breakup is completed within 50 mm distance downstream the atomizer, the drop size and drop velocity measurements were performed with the PDA system at z = 50 mm. Fig. 10 shows the measured drop size distribution at the centerline as an example for the typical droplet size distribution of the nozzle. About 90 % of the droplets have a diameter below 50 µm which is expected due to the high gas velocity at the nozzle orifice (123 m/s) and the low viscosity of the fuel (21 mPa s). Calculated from local drop size

**Table 3**
Elementary composition, ash and water content and lower calorific value (LCV) of the surrogate fuel mono ethylene glycol (MEG) as compared to typical values for pyrolysis oils.

| Mass fraction $Y_i$/wt% | Pyrolysis oil [51,52] | Mono ethylene glycol |
|---|---|---|
| C | 32–49 | 38.5 |
| H | 6–8 | 9.7 |
| O | 44–60 | 51.3 |
| S | 0–0.6 | 0.0 |
| N | – | 0.0 |
| Ash | 0.01–0.2 | 0.0 |
| Water | 15–30 | 0.5 |
| LCV/MJ/kg | 16–19 | 16.6 |

**Table 4**
Set point values of the gasification experiments (REGA-glycol-T1) and the atomization tests at ATMO (for ATMO mass flow rate of fuel, air and oxygen are relevant only).

| | |
|---|---|
| Mass flow rate of fuel $\dot{m}_{fuel}$/kg/h | 12.56 |
| Mass flow rate of air $\dot{m}_{air}$/kg/h[1)] | 9.05 |
| Mass flow rate of oxygen $\dot{m}_{O_2}$/kg/h[1)] | 7.11 |
| Stoichiometric ratio $\lambda_{tech}/\lambda_{abs}$ | 0.57/0.69 |
| Mass flow rate of purge fluid $\dot{m}_{N_2}$/kg/h[1)] | 0.64 |
| Mass flow rate syngas $\dot{m}_{syngas}$/kg/h | 29.4 |
| Adiabatic temperature $T_{ad}$/K | 2273 |
| Average residence time τ ($T_{ad}$)/s | 2.7 |

$T_{ad}$ without dissociation (calculated from equilibrium, Aspen)
[1)] calculated from volume flow rates, see Table 1

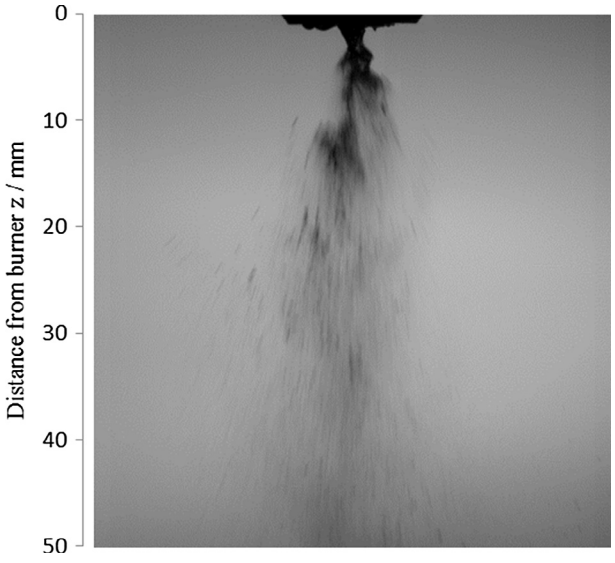


**Fig. 9.** Primary jet breakup and droplet formation for mono ethylene glycol.

distributions, Fig. 11 shows local SMD (left) and mean axial drop velocities values (right) at a position 50 mm downstream the nozzle orifice. The SMD values increase from about 60 µm at the centerline to about 80 µm at 15 mm off axis. The mean axial velocity values reveal a maximum at the centerline (about 60 m/s) and decrease with increasing radial distance (below 15 m/s). Both profiles can be considered as axis-symmetric so that the whole spray can be regarded as rotational symmetric.

The subsequent spray investigations were performed under gasification conditions in REGA gasifier. Again high speed camera measurements were performed close to the nozzle orifice to gather qualitative information about jet breakup, droplet formation and evaporation. Fig. 12 shows the fuel spray during gasification in the near burner region (from the nozzle orifice at z = 0 down to z = 100 mm) by overlapping instantaneous pictures taken at different distances from the burner. Again the liquid jet disintegration takes place directly at the nozzle orifice as it has already been observed in ATMO rig. Despite of the high temperatures close to the burner, droplets are still observed at a distance of 100 mm, showing that liquid fuel is transported well beyond this position.

Finally LDA measurements were performed under gasification conditions to determine radial profiles of local drop velocities at 50 mm downstream of the nozzle orifice. As Fig. 13 shows, the spray angle is wider under gasification conditions (REGA) as compared to ambient conditions (ATMO). The droplet velocities are about 10 m/s larger at the jet axis under gasification conditions as compared to atomization at ambient temperature, thus an increase of about 15 % is observed. This finding may be explained by a volume expansion in the spray due to a temperature increase by entrainment of hot gases from the outer recirculation zone into the spray. In addition, even though the burner is cooled, the atomization medium may have a higher temperature in the gasification experiments due to heat transfer from the reactor to the burner. An increase of 15 % of the exit gas velocity would correspond to a temperature increase of about 40 K.

### 7.3. Global balancing of the REGA gasifier

Table 5 gives the syngas composition measured at the reactor outlet.

Using the set point data and the syngas composition obtained from the global balancing procedure described in Section 5, the following data are obtained:

Mass flow rate of infiltration air $\dot{m}_{infiltration\ air}$: 1.93 kg/h

Water concentration $X_{H_2O}$: 33.08 vol%

Mass flow rate of syngas $\dot{m}_{syngas}$: 31.3 kg/h

Carbon conversion CC: 95.5 %

The global absolute stoichiometry of the process $\lambda_{abs\ global}$ was

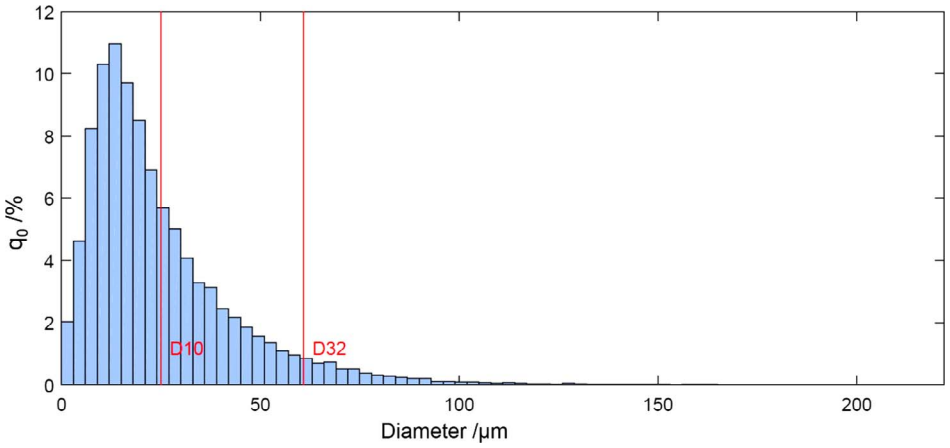


**Fig. 10.** Number based drop size distribution on the centerline of the spray 50 mm downstream the nozzle orifice.

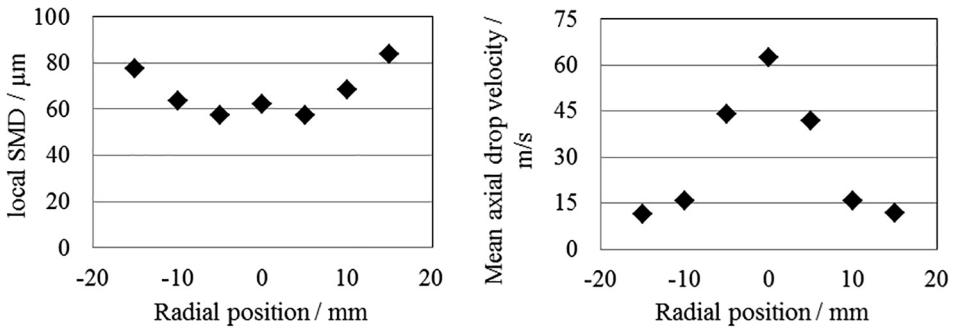


**Fig. 11.** Local SMD (left) and mean axial drop velocity (right) at a distance of 50 mm from the burner nozzle (determined with PDA system).

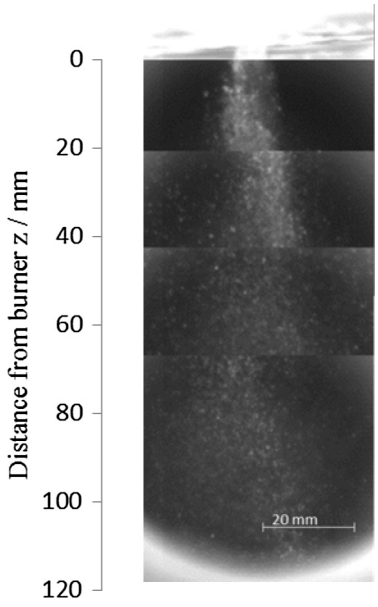


**Fig. 12.** Jet break up and droplet formation for fuel spray during gasification.

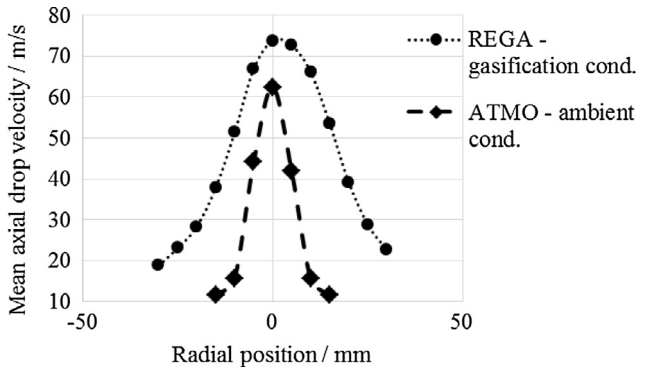


**Fig. 13.** Mean axial droplet velocity at a distance of 50 mm downstream of the burner measured under gasification (REGA) and ambient temperature (ATMO) conditions.

calculated in three ways (see Eqs. (11) and (12)):

- using the feed flow rates and the specifications (see Table 4) 0.69
- as above but including infiltration air 0.71
- using gas species concentrations measured at gasifier exit 0.74

For the temperature at the gasifier outlet two values are determined:

- gas temperature measured $T_{gas,outlet}$ 1369 K,
- TWGS calculated using gas composition measured at gasifier exit 1495 K.

The different values of global absolute stoichiometry show the influence of the infiltration air and incomplete carbon conversion. As

**Table 5**
Gas-phase composition measured at the reactor outlet ($N_2$ calculated according to Eq. (6)).

| | |
|---|---|
| $H_2$/vol%dry | 19.11 |
| CO/vol%dry | 21.86 |
| $CO_2$/vol%dry | 22.05 |
| $CH_4$/vol% dry | 0.013 |
| $N_2$/vol% dry | 36.96 |
| $C_{org}$/g/m$^3$ humid (STP) | 0.026 |

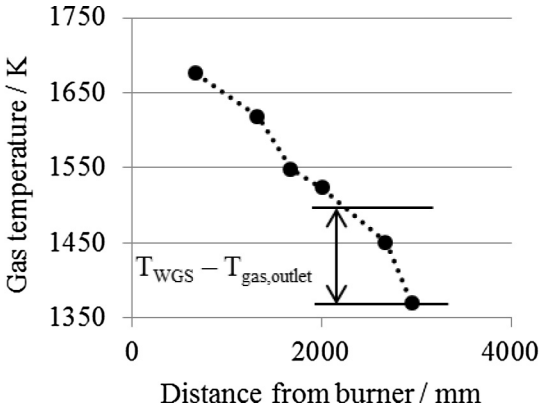


**Fig. 14.** Axial gas temperature profile.

$\lambda_{abs,global}$ = 0.74 (calculated from the gas composition) is higher than $\lambda_{abs,global}$ = 0.71 (calculated using the set point values including the infiltration air) it can be concluded that the glycol is not converted completely into the gas species measured at the reactor outlet.

The temperature measured at the reactor outlet ($T_{gas,outlet}$ = $T_7$ in Fig. 4) is lower by a difference of 126 K as compared to $T_{WGS}$, which indicates that the WGS equilibrium is frozen up-stream of the gasifier exit. From the axial temperature profile (shown in Fig. 14) it can be seen that the WGS reaction equilibrium is reached at approximately z = 2000 mm downstream of the burner.

A global carbon conversion (CC) of 95.5 % is calculated (see Eq. (17)) using the measured data. According to the chemical equilibrium calculations, no hydrocarbons are to be expected for a reactor outlet temperature of 1369 K. The measurements, however, show the presence of hydrocarbons at the reactor outlet at very low concentrations. This is a typical observation also for technical gasifiers. The concentrations of $H_2$, CO, $CO_2$ and $H_2O$ at the reactor outlet are in good agreement with the concentration values obtained from a partial WGS equilibrium calculation for a temperature of 1495 K.

### 7.4. Local profiles in the main reaction zone

Radial profiles of gas-phase composition and temperature, which were measured at 300 and 680 mm distances downstream of the burner, are shown in Fig. 15. The derived gasification parameters ($\lambda_{abs}$, CC and $T_{WGS}$) are also shown in Fig. 16. For additional information the outer contour of the jet is given assuming an expansion angle of 19° [54,55]. The measured species concentrations and values of the characteristic parameters at the reactor outlet are also shown.

The local characteristic parameters showed the effect of infiltration air and purge nitrogen flow both producing a departure of species concentrations and temperature profiles from axis symmetry. This led to a deviation of about 2 % for $\lambda_{abs,\ local}$ and 6 % for $T_{WGS}$, for the positions near the wall. To facilitate comparison with rotationally symmetric numerical simulations presented in the associated papers [14,37] the undisturbed sections of the profiles are used only and are mirrored on the axis.

At a distance of 300 mm the gas species concentrations and the gas temperature show strong non-uniformity. At 680 mm the major species concentrations (besides $CH_4$) and the temperature are almost constant across the reactor cross-section. From 680 mm distance to the reactor outlet $CH_4$ is decomposed further; whereas the major species are shifted to a WGS equilibrium corresponding to 1495 K temperature, i.e. the equilibrium is frozen at 1495 K temperature since a rapid cooling of the gases occurs at the reactor bottom.

As described in detail in Section 2 the characteristic flow pattern in REGA is dominated by the high momentum of the central gas flow, i.e. the gasification medium flow, generating a highly turbulent axis symmetric enclosed jet with an outer recirculation zone carrying hot syngas

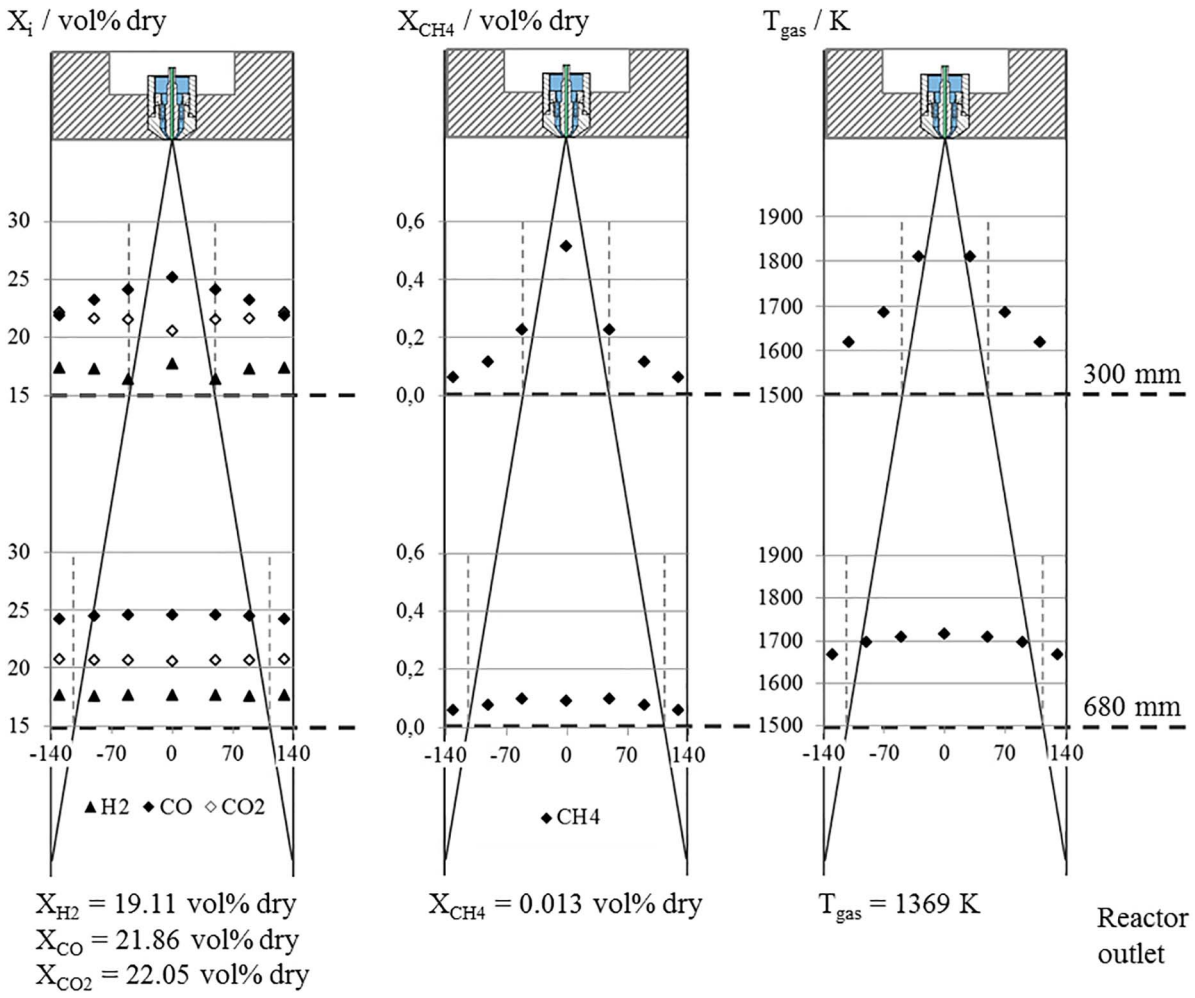


**Fig. 15.** Radial profiles of gas-phase composition and temperature 300 and 680 mm downstream of the burner; boundary of free turbulent jet = continuous line.

from the gasifier exit to the burner zone. It is clear that the flow field with the recirculation zone has a major influence on both the thermochemical processes of gasification and the flame stabilization.

As shown in Fig. 15, at 300 mm distance from the burner $H_2$, CO and $CH_4$ show maxima on the reactor axis, whereas $CO_2$ has a minimum, i.e. local stoichiometry on the jet axis is lower as compared to the overall stoichiometry. This is consistent with the visible observation of the spray (see Fig. 12) which clearly shows fuel droplets at a distance of 120 mm downstream of the burner nozzle. The local stoichiometry $\lambda_{abs,local}$ (see Fig. 16), which is calculated from the measured concentrations, shows a lower value on the axis as compared to the outer recirculation zone; a lower stoichiometry implies a lower temperature. The measured temperatures (see Fig. 15) show the highest value at the outer contour of the jet; at this position a local maximum for $\lambda_{abs,\ local}$ is found. Near the burner nozzle, at the outer contour of the jet, the recirculated syngas reacts with oxygen from the gasification medium and the reactions proceed under oxygen rich conditions, stabilizing the flame. As can be seen in Fig. 16, the measured temperatures are in good agreement with $T_{WGS}$ in the outer recirculation zone up to the outer jet contour. The calculated $T_{WGS}$ shows the expected minimum at the jet axis. The concentration profiles for $CO_2$, CO and $H_2$ are consistent with this observation.

In the outer recirculation zone the gas phase compositions at 300 and 680 mm are similar, as syngas from downstream is transported upwards in the recirculation zone. The temperature, however, is lower near the wall at 300 mm as compared to 680 mm, due to some heat loss through the reactor wall in the upper part of the reactor.

As shown in Fig. 16, at 300 mm distance, the carbon conversion (CC) shows a maximum in the jet, a minimum at the jet boundary and again higher values – similar to those observed at 680 mm – in the recirculation zone. Taking into consideration the opposite trend of the local stoichiometry, it is obvious that the mixing of the reactants is not completed in the jet.

Total organic carbon was measured using an FID-analyzer to examine whether other hydrocarbons besides methane might be present. Fig. 17 shows a comparison of the measured concentrations of organic carbon $C_{org}$ and $CH_4$. The measured $CH_4$ values are converted into g/m$^3$ for reason of comparability. On the jet axis at z = 300 mm, about half of the organic carbon measured using the FID is $CH_4$. At 680 mm distance the amount of organic carbon is lowered by a factor of 10 as compared to 300 mm. Only $CH_4$, as the most stable hydrocarbon, is found in the gas-phase at this position.

## 8. Conclusion

The paper reports on a measurement campaign (named REGA-glycol-T1) concerning gasification of glycol in the Research Entrained flow GAsifier (REGA) operated at atmospheric pressure. The gasifier was operated with mono ethylene glycol, MEG, as a surrogate fuel for bio-oil at a fuel flow rate of 12.5 kg/h, using an oxygen-nitrogen mixture as gasification medium at a global stoichiometry of $\lambda_{abs,global} = 0.74$. The objective of this work was twofold: (a) to gain an insight into the gasification process by carrying out in-gasifier measurements of temperature and gas composition ($H_2$, CO, $CO_2$, $CH_4$, organic carbon) as well as droplet velocity and diameter, (b) to generate a set of consistent data for both the development of mathematical models

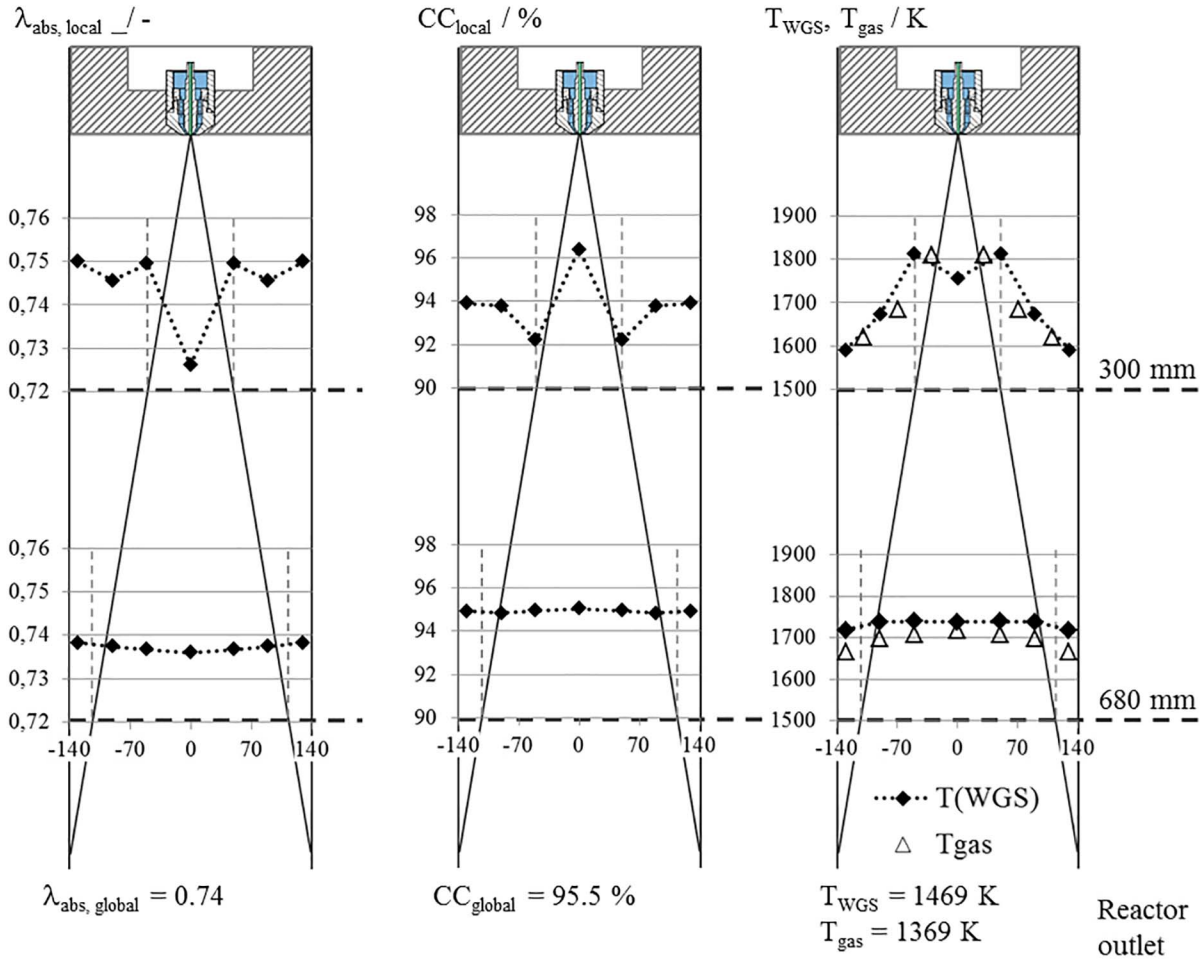


**Fig. 16.** Results from local balancing at 300 and 680 mm downstream of the burner; boundary of free turbulent jet = continuous line.

for gasification sub-processes and the validation of CFD-based mathematical models.

The spray pattern is described by spray angle, droplet size distribution and mean droplet velocity. The overall gasification process is characterized by concentration and temperature measurements at the gasifier outlet. Local concentration of species (CO, $CO_2$, $H_2$ and $CH_4$) and temperature are measured at z = 300 and 680 mm (i.e. $z/d_{eq}$ = 46 and 104) downstream of the burner. Major emphasis has been put on the validation of the experimental data using global and local species balances. Characteristic parameters, i.e. absolute stoichiometry ($\lambda_{abs}$), carbon conversion (CC) and water gas shift temperature ($T_{WGS}$) derived from measured data are reported as local profiles.

The in-gasifier data has identified the existence of several distinct reaction zones: the central spray zone near the burner, where fuel droplets are being produced and evaporated, reaches to about 150 mm ($z/d_{eq}$ = 23) downstream of the burner. The spray zone is enveloped by a high temperature reaction zone which is located at the boundary between the forward flow of the central jet and the strong outer recirculation zone. The recirculation zone extends down to 800 mm distance ($z/d_{eq}$ = 122) transporting hot syngas back to the burner. The syngas, entrained into the gasification medium jet, reacts with oxygen at locally oxygen-rich (combustion) conditions.

At 300 mm distance ($z/d_{eq}$ = 46) the radial profiles of gas temperature and gas composition and of the derived characteristic parameters show strong non-uniformity. At 680 mm ($z/d_{eq}$ = 104) the profiles are flattened out. The gas temperature at the gasifier exit (z/

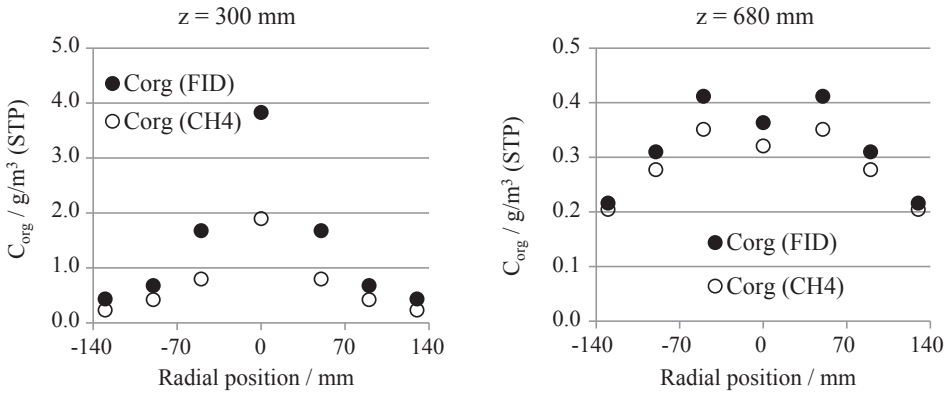


**Fig. 17.** Amount of organic carbon measured with FID ($C_{org}$ (FID)), calculated from NDIR $CH_4$ measurement ($C_{org}$ ($CH_4$)) 300 and 680 mm downstream of the burner.

$d_{eq}$ = 460) is 1369 K, the syngas composition however corresponds to water gas shift reaction equilibrium at 1495 K, which is reached at z/$d_{eq}$ = 306. In other words, the rapid cooling at the gasifier bottom freezes the reactions. Traces of methane (0.01 % wet) and higher hydrocarbons (organic carbon) in amounts of 0.026 g/$m^3$ (STP) have been detected at the gasifier exit.

The REGA-glycol-T1 data set has been produced for the mathematical modelling and to this end emphasis has been placed on producing consistent data (see Appendix A). The procedures for checking the data consistency and inaccuracy have been described in the text.

## Acknowledgements

The authors gratefully acknowledge the financial support by the Helmholtz Association of German Research Centres (HGF) in the frame of the Helmholtz Virtual Institute for Gasification Technology HVIGasTech (VH-VI-429).

## Appendix A

Consolidated inputs and outputs of the REGA-glycol-T1 gasification experiment

**Table A1**
Gasifier inputs.

| Input | Mass flow rate/kg/h | Remarks |
|---|---|---|
| Glycol | 12.56 | Measured with accuracy ± 0.04 kg/h |
| Gasification medium | | |
| Oxygen | 9.22 | Accuracy: see volume flow rates of oxygen and air in Table 1 |
| Nitrogen | 6.94 | |
| Purge nitrogen | 0.64 | Calculated from measured volume flow rate, accuracy ± 0.0005 kg/h |
| Infiltration air | | |
| Oxygen | 0.45 | Calculated using C, H, N, O balances |
| Nitrogen | 1.48 | Calculated using C, H, N, O balances |
| Σ | 31.29 | |

**Table A2**
Syngas leaving REGA (syngas temperature at the gasifier exit = 1369 K).

| Species | Volume fraction vol% wet | Mass flow rate kg/h | Remarks |
|---|---|---|---|
| $H_2$ | 12.79 | 0.34 | Volume fraction measured dry |
| CO | 14.63 | 5.36 | Volume fraction measured dry |
| $CO_2$ | 14.76 | 8.49 | Volume fraction measured dry |
| $CH_4$ | 0.009 | 0.0018 | Volume fraction measured dry |
| $H_2O$ | 33.08 | 7.79 | Calculated using C, H, N, O balances |
| $N_2$ | 24.74 | 9.06 | Volume fraction dry calculated (Eq. (6)) |
| Σ | | 31.04 | |

## References

[1] Higman C. State of the gasification industry – The updated worldwide gasification database. Gasification Technologies Conference, Colorado, Springs, CO, Oct 16, 2013 2013.
[2] DOE National Energy Technology Laboratory. Gasification Plant Databases; Available from: http://www.netl.doe.gov/research/coal/energy-systems/gasification/gasification-plant-databases.
[3] Dahmen N, Abeln J, Eberhard M, Kolb T, Leibold H, Sauer J, Stapf D, Zimmerlin B. The bioliq process for producing synthetic transportation fuels. WIREs Energy Environment (Wiley Interdisciplinary Reviews: Energy and Environment) 2016.
[4] Kolb T, Aigner M, Kneer R, Müller M, Weber R, Djordjevic N. Tackling the challenges in modelling entrained-flow gasification of low-grade feedstock. J Energy Inst 2016;89(4):485–503.
[5] Jakobs T, Djordjevic N, Saenger A, Zarzalis N, Kolb T. Influence of reactor pressure on twin-fluid atomization: Basic investigations on burner design for high-pressure entrained flow gasifier. Atomization Sprays 2015;25(12):1081–105.
[6] Stoesser P, Ruf J, Gupta R, Djordjevic N, Kolb T. Contribution to the understanding of secondary pyrolysis of biomass-based slurry under entrained-flow gasification Conditions. Energy Fuels 2016;30(8):6448–57.
[7] Wu G, Yazhenskikh E, Hack K, Müller M. Viscosity model for oxide melts relevant to fuel slags. Part 2: The system SiO2–Al2O3–CaO–MgO–Na2O–K2O. Fuel Process Technol 2015;138:520–33.
[8] Alberti M, Weber R, Mancini M. Re-creating Hottel's emissivity charts for carbon dioxide and extending them to 40 bar pressure using HITEMP-2010 data base. Combust Flame 2015;162(3):597–612.
[9] Alberti M, Weber R, Mancini M, Fateev A, Clausen S. Validation of HITEMP-2010 for carbon dioxide and water vapour at high temperatures and atmospheric pressures in 450–7600 $cm^{-1}$ spectral range. J Quant Spectrosc Radiat Transfer 2015;157:14–33.
[10] Nilsson B. Gasification of carbonaceous material in a reactor having a gasification zone and a combustion zone(US5486269 A); 1996.
[11] Whitty K. Investigation of pressurized entrained-flow Kraft black liquor gasification in an industrially relevant environment: Final Technical Report (DOE Coop. Agreement DE-FC26-04NT42261); 2007.
[12] Jakobs T, Djordjevic N, Fleck S, Mancini M, Weber R, Kolb T. Gasification of high viscous slurry R&D on atomization and numerical simulation. Appl Energy 2012;93:449–56.
[13] Mansour A, Chigier N. Air-blast atomization of non-Newtonian liquids. J Nonnewton Fluid Mech 1995;58:161–94.
[14] Mancini M, Alberti M, Dammann M, Santo U, Weber R, Kolb T, Eckel G. Entrained Flow Gasification Part 2: Mathematical modeling of the gasifier using RANS method. submitted to Fuel 2017.
[15] Mueller A, Haustein HD, Stoesser P, Kreitzberg T, Kneer R, Kolb T. Gasification kinetics of biomass- and fossil-based fuels: comparison study using fluidized bed and thermogravimetric analysis. Energy Fuels 2015;29(10):6717–23.
[16] Stoesser P, Schneider C, Kreitzberg T, Kneer R, Kolb T. Comparison of reaction systems for the establishment of heterogeneous gasification kinetics. submitted to Applied Energy; 2017.
[17] Chen C, Horio M, Kojima T. Numerical simulation of entrained flow coal gasifiers. Part I: modeling of coal gasification in an entrained flow gasifier. Chem Eng Sci 2000;55(18):3861–74.
[18] Chen C, Horio M, Kojima T. Numerical simulation of entrained flow coal gasifiers. Part II: effects of operating conditions on gasifier performance. Chem Eng Sci 2000;55(18):3875–83.
[19] Guo X, Dai Z, Gong X, Chen X, Liu H, Wang F, et al. Performance of an entrained-flow gasification technology of pulverized coal in pilot-scale plant. Fuel Process

Technol 2007;88(5):451–9.
[20] Harris DJ, Roberts DG, Henderson DG. Gasification behaviour of Australian coals at high temperature and pressure. Fuel 2006;85(2):134–42.
[21] Brown B, Smoot LD, Smith PJ, Hedman PO. Measurement and prediction of entrained-flow gasification processes. AlChE J 1988;34(3):435–46.
[22] Soelberg NR, Smoot LD, Hedman PO. Entrained flow gasification of coal: 1. Evaluation of mixing and reaction processes from local measurements. Fuel 1985;64:776–81.
[23] Azuhata S, Hedman PO, Smoot LD. Carbon conversion in an atmospheric-pressure entrained coal gasifier. Fuel 1986;65:212–7.
[24] Smoot LD, Brown BW. Controlling mechanism in gasification of pulverized coal. Fuel 1987;66(9):1249–56.
[25] Kumar M, Ghoniem AF. Multiphysics simulations of entrained flow gasification. Part II: constructing and validating the overall model. Energy Fuels 2012;26(1):464–79.
[26] Vascellari M, Arora R, Hasse C. Simulation of entrained flow gasification with advanced coal conversion submodels. Part 2: char conversion. Fuel 2014;118:369–84.
[27] Tremel A, Haselsteiner T, Kunze C, Spliethoff H. Experimental investigation of high temperature and high pressure coal gasification. Appl Energy 2012;92:279–85.
[28] Qin K, Lin W, Jensen PA, Jensen AD. High-temperature entrained flow gasification of biomass. Fuel 2012;93:589–600.
[29] Hernández JJ, Aranda-Almansa G, Bula A. Gasification of biomass wastes in an entrained flow gasifier: effect of the particle size and the residence time. Fuel Process Technol 2010;91(6):681–92.
[30] Qin K. Entrained flow gasification of biomass. Lyngby: Technical University of Denmark (DTU); 2012. [Ph.D. Thesis].
[31] Ku X, Li T, Løvås T. Eulerian-Lagrangian simulation of biomass gasification behavior in a high-temperature entrained-flow reactor. Energy Fuels 2014;28(8):5184–96.
[32] Sricharoenchaikul V, Agrawal P, Frederick WJ. Black liquor gasification characteristics. 1. Formation and conversion of carbon-containing product gases. Ind Eng Chem Res 2002;41(23):5640–9.
[33] Carlsson P, Wiinikka H, Marklund M, Grönberg C, Pettersson E, Lidman M, et al. Experimental investigation of an industrial scale black liquor gasifier. 1. The effect of reactor operation parameters on product gas composition. Fuel 2010;89(12):4025–34.
[34] Weiland F, Wiinikka H, Hedman H, Wennebro J, Pettersson E, Gebart R. Influence of process parameters on the performance of an oxygen blown entrained flow biomass gasifier. Fuel 2015;153:510–9.
[35] Carlsson P, Iisa K, Gebart R. Computational fluid dynamics simulations of raw gas composition from a Black Liquor gasifier—Comparison with experiments. Energy Fuels 2011;25(9):4122–8.
[36] Marklund M. Pressurized entrained-flow high temperature Black Liquor gasification: CFD based reactor scale-up method and spray burner characterization. Luleå University of Technology; 2006. [PhD Thesis].
[37] Eckel G, Le Clercq PC, Kathrotia T, Saenger A, Fleck S, Mancini M, Kolb T, Aigner M. Entrained flow gasification. Part 3: Insight into the reactor near-field by Large Eddy Simulation with detailed chemistry. submitted to Fuel; 2017.
[38] Lackner M, Winter F, Agarwal AK. Handbook of Combustion. Weinheim, Germany: Wiley-VCH Verlag GmbH & Co. KGaA; 2010.
[39] Beér JM, Thring MW (eds.). Industrial Flames: Measurement in Flames. Edward Arnold (Publishers) Ltd; 1972.
[40] Sänger A, Jakobs T, Djordjevic N, Kolb T. Effect of primary instability of a high viscous liquid jet on the spray quality generated by a twin-fluid atomizer. In: 26th Annual Conference on Liquid Atomization and Spray Systems – ILASS Europe; Bremen, Germany; 2014.
[41] Albrecht HE. Laser Doppler and Phase Doppler Measurement Techniques. Berlin, New York: Springer; 2003.
[42] Kapulla R, Najera SB. Operation conditions of a phase Doppler anemometer: Droplet size measurements with laser beam power, photomultiplier voltage, signal gain and signal-to-noise ratio as parameters. Meas Sci Technol 2006;17(1):221–7.
[43] Hiller H, Reimert R, Stoenner H-M. Gas Production, 1. Introduction. In: Ullmann's encyclopedia of industrial chemistry, Weinheim, Germany: Wiley-VCH Verlag GmbH & Co. KGaA; 2000.
[44] Evans RJ, Milne TA. Molecular characterization of the pyrolysis of biomass. 1. Fundamentals. Energy Fuels 1986;2:123–37.
[45] Ortwein A. Modellierung der Hochdruck-Partialoxidation von Heiz- und Schweröl [Dissertation]. Freiberg: Technische Universität Bergakademie Freiberg; 2011.
[46] Burgt Higman C. Maarten van der. Gasification. Boston: Elsevier/Gulf Professional Pub; 2003.
[47] Brueggemann P. Formation and evolution of by-products and trace substances in the high pressure partial oxidation of gaseous and liquid hydrocarbons [Dissertation]. Freiberg: Technische Universität Bergakademie Freiberg; 2010.
[48] Vejahati F, Katalambula H, Gupta R. Entrained-flow gasification of oil sand coke with coal: assessment of operating variables and blending ratio via response surface methodology. Energy Fuels 2012;26(1):219–32.
[49] Cousins A, McCalden DJ, Hughes RW, Lu DY, Anthony EJ. Entrained-flow gasifier fuel blending studies at pilot scale. Can J Chem Eng 2008;86(3):335–46.
[50] Smith GP, Golden DM, Frenklach M, Moriarty NW, Eiteneer B, Goldenberg M, Bowman CT, Hanson RK, Song S, William J, Gardiner C, Lissianski VV, Qin Z. GRI mechanism 3.0. Tech. Rep., Sandia National Laboratories; 2000.
[51] Kaltschmitt M. Energie aus Biomasse: Grundlagen, Techniken und Verfahren. 2nd ed. Dordrecht, Heidelberg, London, New York, NY: Springer; 2009.
[52] Basu P. Biomass Gasification and Pyrolysis: Practical Design and Theory. Amsterdam: Elsevier Inc; 2010.
[53] Chigier NA, Farago Z. Morphological classification of disintegration of round liquid jets in a coaxial air stream. Atomization Sprays 1992:137–53.
[54] Beér JM, Chigier NA. Combustion aerodynamics. Robert E. Krieger Publishing Company, Inc; 1972.
[55] Thring MW, Newby MP. Combustion length of enclosed turbulent jet flames. Symp (Int) Combust 1953;4(1):789–96.